Supplemental Information

PXRD of NCA hydroxide precursor.

Figure S1 shows the powder XRD pattern of the NCA hydroxide precursor that forms from the initial coprecipitation reactions. Subsequent processing steps using the molten salt method convert this hydroxide into the oxide used for the studies here.

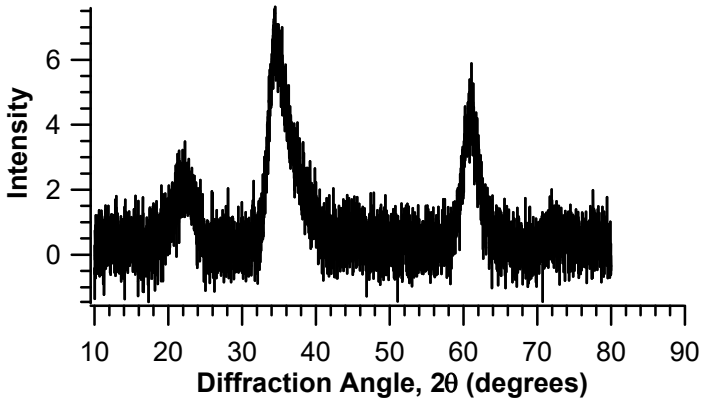

Figure S1: Powder XRD pattern of the NCA hydroxide synthesized using a coprecipitation reaction.

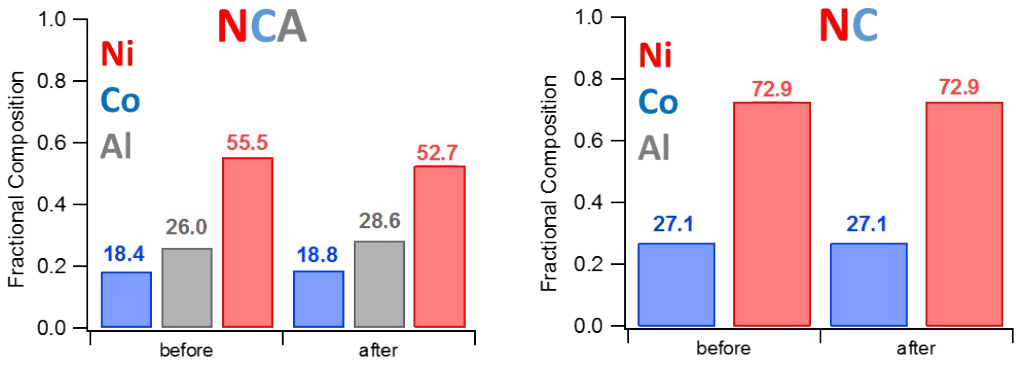

Figure S2: XPS analysis of nanoparticle surfaces before and after incubation in moderately hard reconstructed water (MHRW).
Fractional composition of metal species at the surface of NC and NCA nanoparticles before and after 72 h incubation in MHRW for 72 h. 50 mg/L nanoparticles were incubated in medium and then washed with nanopure water three times prior to XPS analysis. Fractional composition is shown for (**f**) Ni and Co in NC and (**g**) Ni, Co and Al in NCA.

XPS of NC(A) in MHRW

Fractional composition X_i for different elements *i* was calculated as:

$$X_i = \frac{\frac{A_i}{S_i}}{\sum_j \frac{A_j}{S_j}}$$

where A_i refers to the XPS peak area of element i, S_i is the atomic sensitivity factor for element *i*, and the sum in the denominator is taken over Al, Co, and Ni only. This fractional composition is a semiquantitative measure of the amount of each metal detected at the nanoparticle surface but has systematic errors because it does not take into account the different inelastic mean free paths of photoelectrons from the different elements. Notably, since Al has a high photoelectron energy, the calculated fractional compositions overestimate the amount of Al in the materials. Despite this systematic error, changes in the compositions due to exposure to different media would still be expected to be qualitatively correct.

XPS of NC(A) in Minimal Media

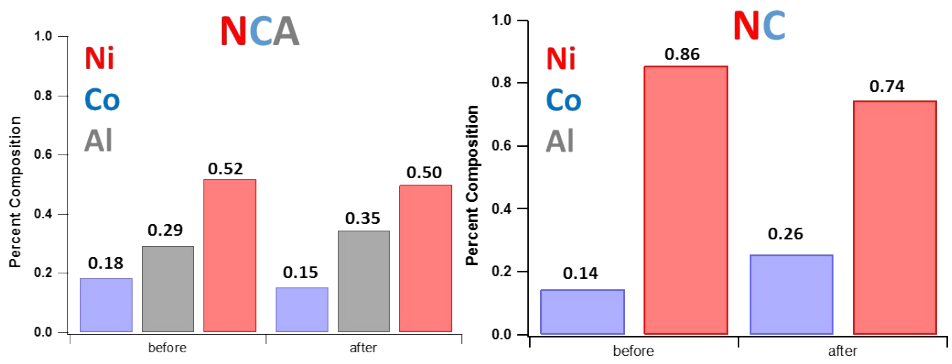

Figure S3: XPS analysis of nanoparticle surfaces before and after incubation in minimal medium (MM). Fractional composition of metal species at the surface of NC and NCA nanoparticles before and after 72 h incubation in MM for 72 h. 50 mg/L nanoparticles were incubated in medium and then washed with nanopure water three times prior to XPS analysis. Fractional composition is shown for (**f**) Ni and Co in NC and (**g**) Ni, Co and Al in NCA.

NC(A) Surface Models

NC-NN-1

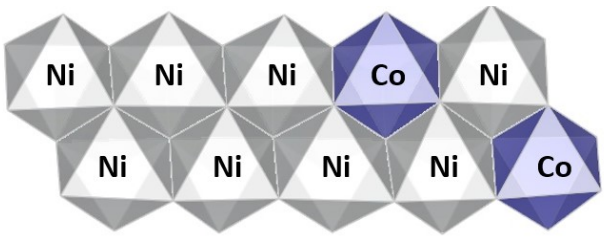

NC-NN-2

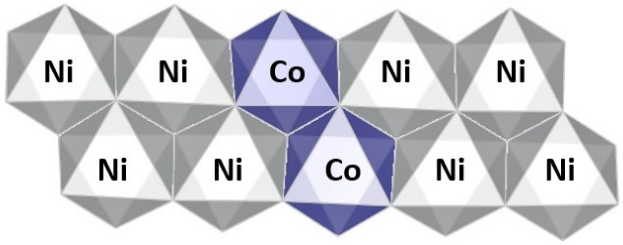

NC-nNN

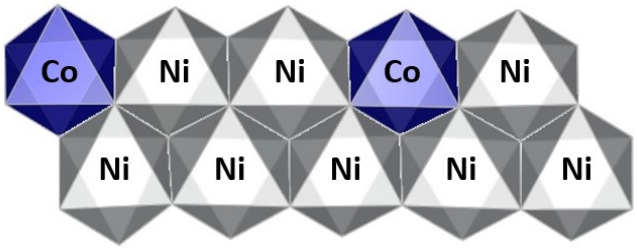

NCA-NN-1

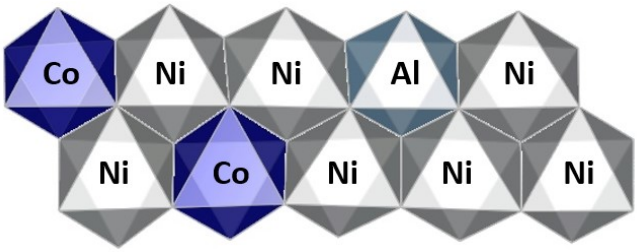

NCA-NN-2

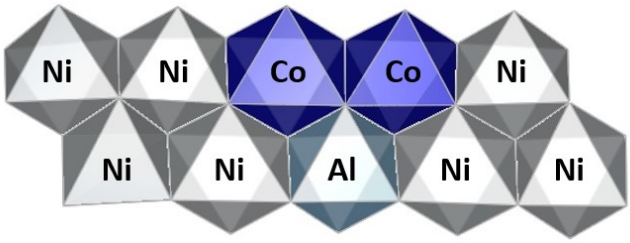

NCA-NN-3

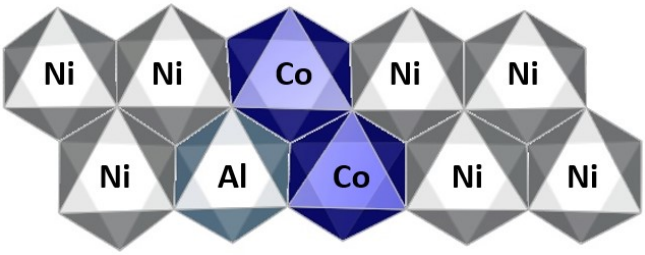

NCA-nNN

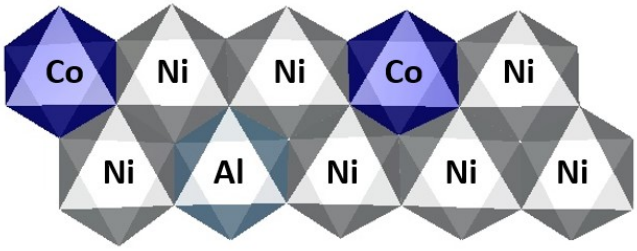

Figures S4: Top-down views of NC(A) surface models with Ni, Co, and Al shown as grey, dark blue, and light blue polyhedron, respectively.

Layer Spacing Comparison between NC and NCA

Table S1: O-Li-O and O-M-O comparisons between NN and nNN configurations for NC and NCA models.

	NC-NN	NCA-NN	% Change	NC-nNN	NCA-nNN	% Change
O-Li-O (Å)	2.65	2.66	0.38	2.65	2.66	0.25
O-M-O (Å)	2.09	2.08	-0.48	2.09	2.08	-0.37

Examining our NC and NCA models we observed no significant structural changes. Our model uses a composition of NCA with 10% Al which is on the high end of dopant amount suggesting anything less would also not have a large change on the structure of the parent NC material.

DFT + Solvent Ion Model

This approach breaks down the energy of a total reaction, ΔG_T, into two groups of terms. The first group of terms term is determined entirely using DFT total energy values, with corresponding changes in energy denoted as ΔG_1. As in previous work[54], we go from DFT total energies to Gibbs free energies using zero-point energy and TΔS corrections. Based on the following model reactions, we represent the removal of an *M*-OH unit, where *M* = Ni, Al, or Co, from the lattice. This release unit has shown to be the favorable leaving group in previous studies and the approach is adopted here.

Eq S1. $$\Delta G_1: E(LiMO_2)_{Ni-OH} \rightarrow E(LiMO_2)\_\_\_ + E(Ni_{(s)}) + E(\frac{1}{2}O_{2\,(g)}) + E(\frac{1}{2}H_{2\,(g)})$$

In this fashion, ΔG_1 can be interpreted as the energy penalty to remove the *M-OH* unit from the lattice, where a more negative value represents a more favorable process. We can systematically vary chemical environments between NC and NCA to determine the effects of aluminum doping on the release process. For example, in this work we compare Ni removal from NC where a neighboring Ni atom is replaced with Al in NCA.

The values for the second group of terms in the DFT Solvent Ion model, ΔG_2, are obtained from tabulated values of ΔG^0_{SHE} with additional correction terms for pH and concentration based on

the Nernst equation as shown in **Eq. S2**. The additional terms allow us to tune our model to relate our calculations better to the environmental conditions of the dissolution experiment.

Table S2: SHE values for the solvation of the solid metals to their aqueous cations.

(eV)	Co^{2+}	Ni^{2+}	Al^{3+}
ΔG°_{SHE}	-0.56	-0.47	-5.03

Eq S2
$$\Delta G_2 = \Delta G^{0}_{SHE} - n_e e U_{SHE} - 0.0591\, n_H pH + 0.0257\, ln\, a\,(H_x AO^{z-}_{y})$$

ΔG^{0}_{SHE} accounts for the free energy change upon hydrolysis of the standard state products in ΔG_1 in reference to the Standard Hydrogen Electrode (SHE).

Eq S3
$$\Delta G^{0\,Ni}_{SHE}: Ni_{(s)} \rightarrow Ni^{2+}_{(aq)} + 2e^-$$

Eq S4
$$\Delta G^{0\,H}_{SHE}: \frac{1}{2} H_{2\,(g)} \rightarrow H^{+}_{(aq)} + e^-$$

Eq S5
$$\Delta G^{0\,O}_{SHE}: \frac{1}{2} O_{2\,(g)} + 2e^- + 2H^{+}_{(aq)} \rightarrow H_2O_{(l)}$$

The media-dependent dissolution results suggest that reactions in solution may thermodynamically promote or hinder cation release in a metal-dependent fashion. To this end, we modeled the energetics of ligand exchange reactions involving the hydrated cation forms of released metals and known chelating species present in the media. These aqueous chemistry effects on the release were modeled using molecular (non-periodic) DFT calculations at the GGA-PBE level of theory using DMol^3 software.[57, 58] DNP basis functions were used to expand the Kohn-Sham orbitals[59] on a fine numerical integration grid. Using the conductor-like screening model (COSMO) as implemented in the DMol^3 package,[60] an implicitly solvated aqueous environment was modeled.

The solution effects add on to the DFT Solvent-Ion framework as elementary steps that result in the formation of complexed metal ions, which introduces an additional term denoted as ΔG_3. ΔG_3 is the sum of the energetics of products minus those of reactants for the ligand exchange

reaction between the hydrolyzed metal and the ligating species present in the media **(Eq S6.6-7).**

Eq S6 $$\Delta G_3^M: G[M(H_2O)_6]_{(aq)}^{2+} + G(2LA^-)_{(aq)} \rightarrow G[M(LA)_2(H_2O)_2]_{(aq)} + G(4H_2O)_{(aq)}$$

Al leaves in Al^{3+} state, thus its equation differs by a positive charge. For Al, the reaction was modeled as:

Eq S7 $$\Delta G_3^{Al}: G[Al(H_2O)_6]_{(aq)}^{3+} + G(2LA^-)_{(aq)} \rightarrow G[Al(LA)_2(H_2O)_2]_{(aq)}^{+} + G(4H_2O)_{(aq)}$$

In a previous study on the Ni-enriched 811-NMC,[56] it was shown that a bi-lactate ligated form of Ni and Co is more energetically favorable than the mono-lactate ligated complex. For comparison, we assumed the same degree of ligation for Al. Our bi-lactate ligated metals are all *trans* isomers as this isomer was more stable than the *cis* isomer.

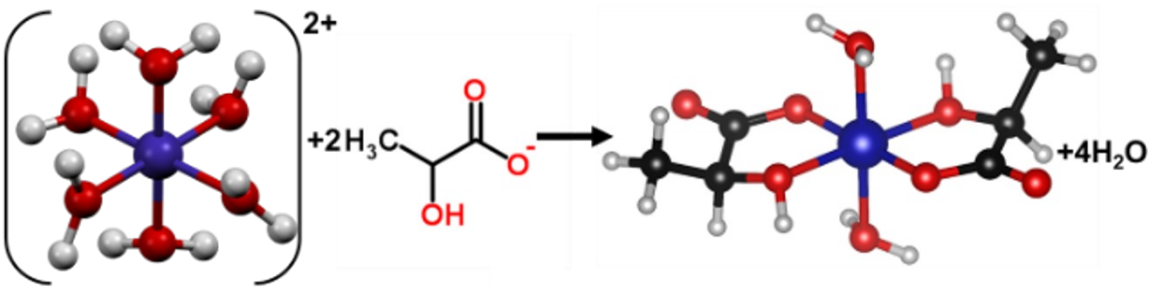

Figure S5: ΔG_3 reaction for hexa-aqua ligated cation undergoing a ligand exchange with lactate to form the *trans* isomer.

ΔG_T Tables for *M*-OH Release

Table S3: ΔG_T for NC at pH 7 for Ni and Co and their differences with and without lactate.

NC	ΔG_T (eV)	$\Delta(\Delta G_T)$ (eV)	$\Delta G'_T$ (eV)	$\Delta(\Delta G'_T)$ (eV)
NN-A-Ni$^{5Ni-1Co}$	-3.75	1.21	-4.71	0.80
NN-A-Co$^{5Ni-1Co}$	-2.54		-3.91	
NN-B-Ni$^{3Ni-3Co}$	-3.36	0.75	-4.32	0.34
NN-B-Co$^{5Ni-1Co}$	-2.61		-3.98	
NN-C-Ni$^{4Ni-2Co}$	-2.99	0.72	-3.95	0.31
NN-C-Co$^{4Ni-2Co}$	-2.27		-3.64	
nNN-A-Ni$^{4Ni-2Co}$	-3.55	0.58	-4.51	0.17
nNN-A-Co^{6Ni}	-2.97		-4.34	

Table S4: ΔG_T for NCA at pH 7 for Ni and Co and their differences with and without lactate.

NCA	ΔG_T (eV)	$\Delta(\Delta G_T)$ (eV)	$\Delta G'_T$ (eV)	$\Delta(\Delta G'_T)$ (eV)
NN-A-Ni$^{4Ni-2Al}$	-3.05	0.59	-4.01	0.18
NN-A-Co$^{5Ni-1Co}$	-2.46		-3.83	
NN-B-Ni^{6Ni}	-4.22	0.86	-5.18	0.45
NN-B-Co$^{4Ni-1Co-1Al}$	-3.36		-4.73	
NN-C-Ni$^{5Ni-1Al}$	-3.33	0.67	-4.29	0.26
NN-C-Co$^{3Ni-2Co-1Al}$	-2.66		-4.03	
nNN-A-Ni$^{4Ni-2Co}$	-3.33	0.66	-4.29	0.25
nNN-A-Co^{6Ni}	-2.67		-4.04	
nNN-A-Ni$^{4Ni-1Co-1Al}$	-3.23	0.56	-4.19	0.15
nNN-A-Co^{6Ni}	-2.67		-4.04	

Table S5: ΔG_T for NCA at pH 4 for Ni and Al and their differences with and without lactate.

NCA	ΔG_T (eV)	$\Delta(\Delta G_T)$ (eV)	$\Delta G'_T$ (eV)	$\Delta(\Delta G'_T)$ (eV)
NN-Ni$^{3Ni-3Co}$	-5.24	1.12	-6.20	0.05

NN-Al^{6Ni}	-4.12		-6.25	
nNN-Ni$^{5Ni-1Al}$	-4.88	1.23	-5.84	0.06
nNN-Al$^{4Ni-2Co}$	-3.65		-5.78	
nNN-Ni$^{4Ni-1Co}$	-4.29	1.03	-5.25	0.14
nNN-Al$^{5Ni-1Co}$	-3.26		-5.39	

TEM Analysis of Nanoparticles

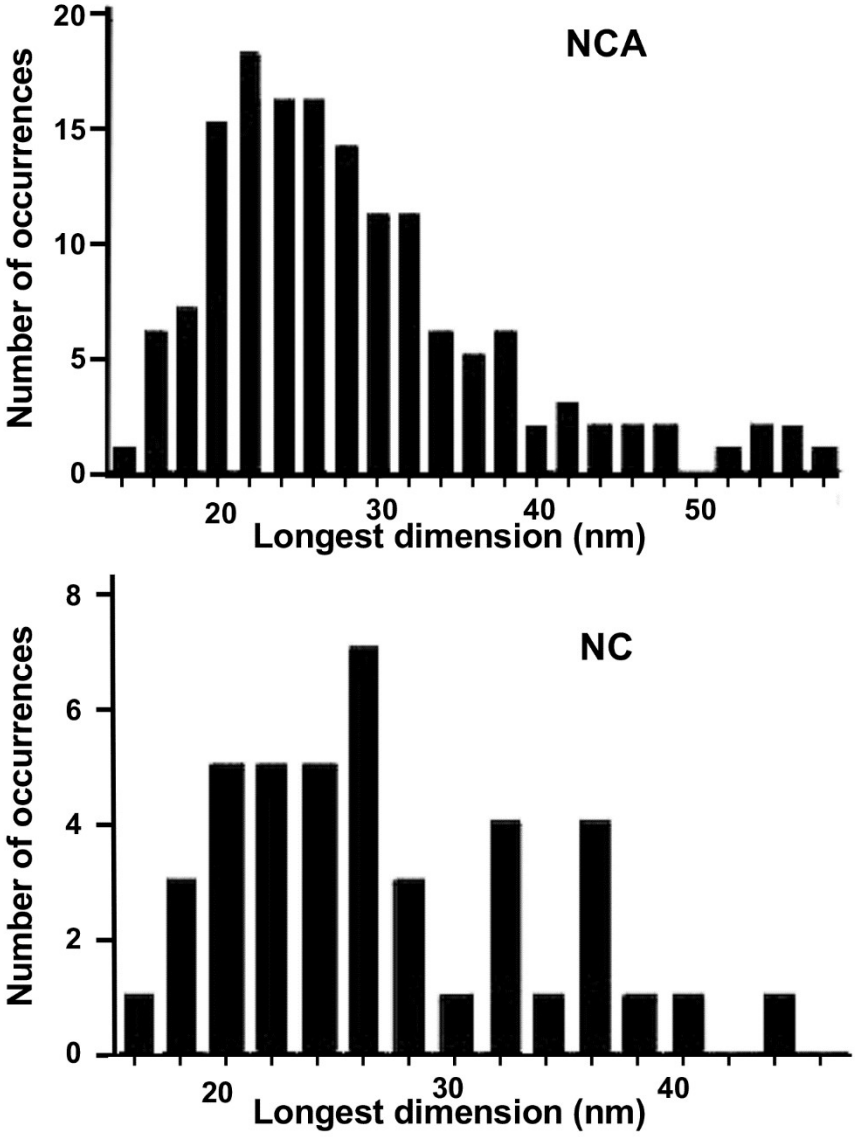

Figure S6: TEM analysis of nanoparticle size distributions for NCA and NC synthesized using the molten salt method at 450°C for 30 min.

Projected Densities of States (PDOS) of Ni in NC and NCA Formulations

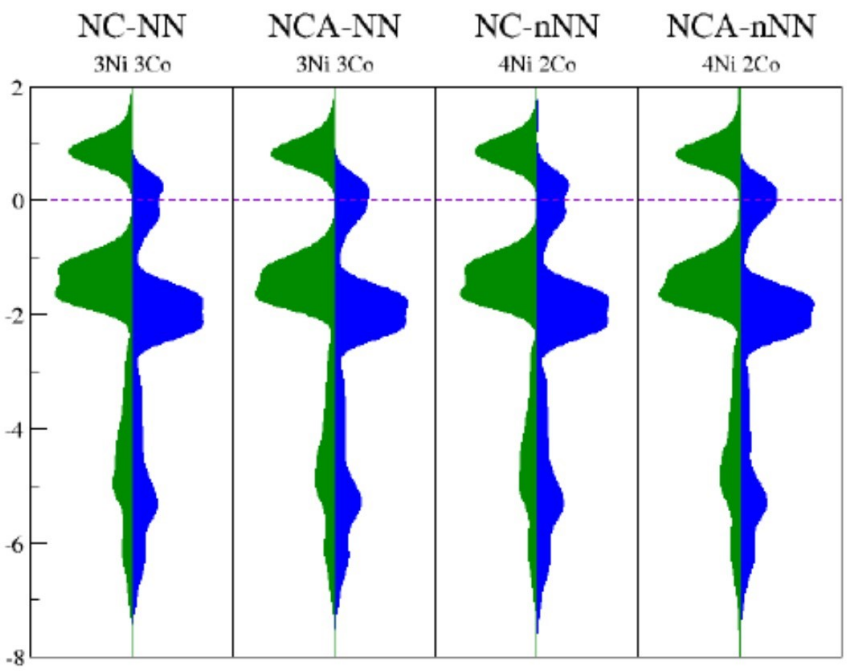

Figure S7: PDOS of Ni in NC and NCA compositions. Ni is present as a 3+ cation in NC with no changes observed after the addition of Al.

Vibrational Mode Comparison between NC and NCA

Table S6: Vibrational mode comparison between NC and NCA. All NCA modes have larger cm^{-1} values indicating the addition of Al strengthens the bonding network.

Mode	NC(cm^{-1})	NCA (cm^{-1})	NCA-NC (cm^{-1})
300	538.976	545.075	6.099
304	542.985	551.973	8.987
305	543.638	552.237	8.598
306	546.195	555.140	8.945
307	546.319	557.058	10.73
316	565.755	568.336	2.581
318	567.652	574.468	6.816
320	572.613	579.592	6.979
322	574.991	585.089	10.09
323	576.102	585.589	9.486
329	591.948	596.720	4.771
332	596.266	603.348	7.082